Implications for the Thin-Film Densification of TiO_2 from Carboxylic Acid-Modified Titanium Alkoxides. Syntheses, Characterizations, X-ray Structures of $Ti_3(\mu_3\text{-}O)(O_2CH)_2(ONep)_8$, $Ti_3(\mu_3\text{-}O)(O_2CMe)_2(ONep)_8$, $Ti_6(\mu_3\text{-}O)_6(O_2CCHMe_2)_6(ONep)_6$, $[Ti(\mu\text{-}O_2CCMe_3)(ONep)_3]_2$, and $Ti_3(\mu_3\text{-}O)(O_2CCH_2CMe_3)_2(ONep)_8$ ($ONep = OCH_2CMe_3$)[1]

Timothy J. Boyle,*,† Ryan P. Tyner,† Todd M. Alam,‡ Brian L. Scott,§ Joseph W. Ziller,⊥ and B. G. Potter, Jr.||

Contribution from the Advanced Materials Laboratory, Sandia National Laboratories, 1001 University Boulevard SE, Albuquerque, New Mexico 87106, Department of Materials Aging and Reliability, Sandia National Laboratories, Albuquerque, New Mexico 87185-1407, Chemical Science and Technology Division—X-ray Diffraction Laboratory, CST-18, Los Alamos National Laboratories, Los Alamos, New Mexico 87545, X-ray Diffraction Laboratory, Department of Chemistry, University of California—Irvine, Irvine, California 92717, and Electronic & Optical Materials, Sandia National Laboratories, Albuquerque, New Mexico 87185-1405

Received July 16, 1999

Abstract: Carboxylic acid (HORc)-modified $Ti(OR)_4$ products were used to study the effect that similarly ligated species with substantially varied structures have on the final densification of the resultant ceramic (in this case TiO_2). The 1:1 stoichiometric products isolated from the reactions of $[Ti(\mu\text{-}ONep)(ONep)_3]_2$ (**1**, $ONep = OCH_2CMe_3$) and a variety of sterically hindered carboxylic acids [HORc: HOFc (HO_2CH), HOAc (HO_2CCH_3), HOPc (HO_2CCHMe_2), HOBc (HO_2CCMe_3), or HONc ($HO_2CCH_2CMe_3$)] were identified by single-crystal X-ray diffraction and solid-state ^{13}C MAS NMR spectroscopy as $Ti_3(\mu_3\text{-}O)(OFc)_2(ONep)_8$ (**2**), $Ti_3(\mu_3\text{-}O)(OAc)_2(ONep)_8$ (**3**), $Ti_6(\mu_3\text{-}O)_6(OPc)_6(ONep)_6$ (**4**), $Ti_2(\mu\text{-}OBc)_2(ONep)_6$ (**5**), and $Ti_3(\mu_3\text{-}O)(ONc)_2(ONep)_8$ (**6**). Compounds **2**, **3**, and **6** adopt a triangular arrangement of Ti atoms linked by a μ_3-oxide moiety with ORc and ONep ligands supporting the basic framework. Compound **4** adopts a distorted, hexagon-prism geometry of two offset $[Ti-O-]_3$ rings with each six-coordinated metal possessing a terminal ONep and two monodentate OPc ligands. The unique, nonesterified product **5** is dimeric with two μ-ONep, two unidentate bridging OBc, and two terminal ONep ligands. The solution behaviors of **2**−**6** were investigated by NMR experiments and were found to retain the solid-state structure in solution with a great deal of ligand rearrangement. Films of TiO_2 were made from redissolved crystals of **2**−**6**. The highest density TiO_2 thin films were derived from the partially hydrolyzed, trinuclear, low-carbon-containing ONep complexes **2** and **3**, as determined from ellipsometric data.

Introduction

Thin films of ceramic materials are often produced through the use of solution route techniques (i.e., dip- or spin-coating). In general, these processes involve the dissolution of the precursors in a solvent, deposition of the resultant precursor solution onto a substrate, and thermal treatment of the deposited film to convert the metallo-organic species to the ceramic phase. Metal alkoxide precursors are often favored for solution routes due to their high solubility in a variety of solvents, their low decomposition/crystallization temperatures, their ability to "cross-link" upon exposure to ambient atmosphere, and the variety of ligands available.[2−6] However, alkoxide precursors are often *too* reactive, with ambient humidity forming large complex molecules upon exposure.[7−9] Modifications to their ligand sets are therefore required in order to tailor hydrolysis and condensation rates to allow for the production of high-quality thin films.

Multidentate ligands have been used to modify the reactivity of the $Ti(OR)_4$ precursors by decreasing the number of

* To whom correspondence should be addressed.
† Advanced Materials Laboratory, Sandia National Laboratories.
‡ Department of Materials Aging and Reliability, Sandia National Laboratories.
§ Los Alamos National Laboratories.
⊥ University of California—Irvine.
|| Electronic & Optical Materials, Sandia National Laboratories.

(1) Boyle, T. J.; Tyner, R.; Scott, B. L.; Ziller, J. W. *Abstracts of Papers*, 217th National Meeting of the American Chemical Society, Anaheim, CA, Spring 1999; American Chemical Society: Washington, DC, 1999; Part 1, INOR-625.
(2) Bradley, D. C.; Mehrotra, R. C.; Gaur, D. P. *Metal Alkoxides*; Academic Press: New York, 1978.
(3) Bradley, D. C. *Chem. Rev.* **1989**, *89*, 1317.
(4) Hubert-Pfalzgraf, L. G. *New J. Chem.* **1987**, *11*, 663.
(5) Caulton, K. G.; Hubert-Pfalzgraf, L. G. *Chem. Rev.* **1990**, *90*, 969.
(6) Chandler, C. D.; Roger, C.; Hampden-Smith, M. J. *Chem. Rev.* **1993**, *93*, 1205.
(7) Boyle, T. J.; Alam, T. M.; Mechenbeir, E. R.; Scott, B.; Ziller, J. W. *Abstracts of Papers*, 213th National Meeting of the American Chemical Society, San Francisco, CA, Spring 1997; American Chemical Society: Washington, DC, 1999; Part 2, INOR-693.
(8) Day, V. W.; Everspacher, T. A.; Klemperer, W. G.; Park, C. W. *J. Am. Chem. Soc.* **1993**, *115*, 8469.

10.1021/ja992521w CCC: $18.00
Published on Web 12/08/1999

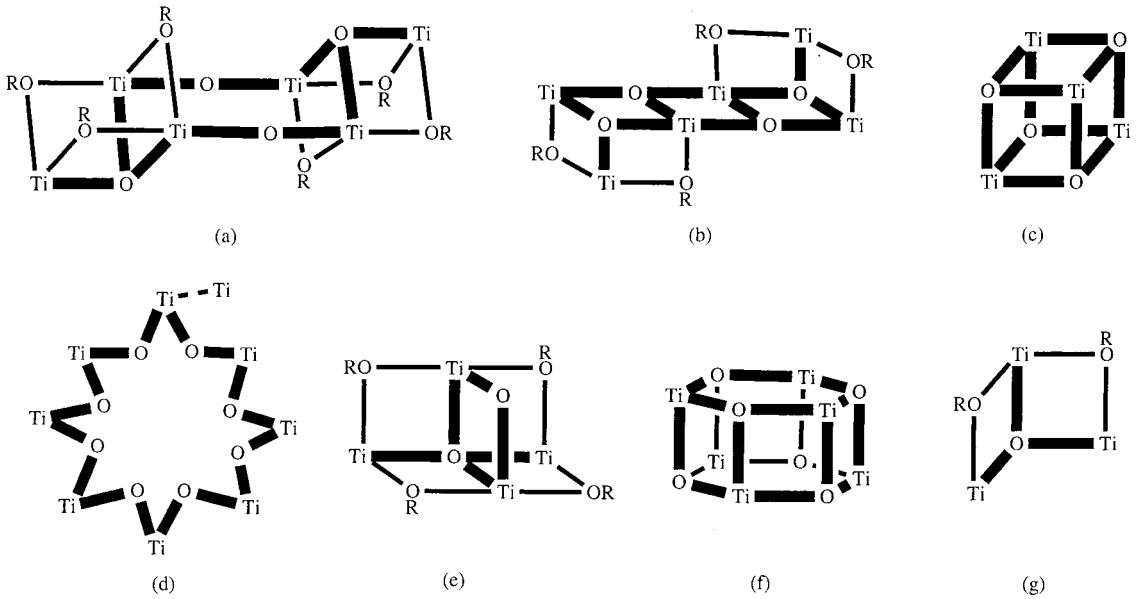

Figure 1. Schematic representations of the skeletal arrangements of titanium oxo, alkoxy, and acetate compounds, referred to as (a) corner-removed, inversion-related, oxide-bridge cube, (b) inversion-related, corner-removed, edge-shared cube, (c) cube, (d) star, (e) face-shared, mirror corner-removed cube, (f) hexagon-prism, and (g) dual corner-missing cube.

hydrolyzable (terminal) ligands.[10−16] One modifier that has gained widespread use is acetic acid (HOAc = HO_2CMe); however, the reaction of $Ti(OR)_4$ with HOAc leads to compounds of the general formula $Ti_6O_4(OAc)_{16-4n}(OR')_{4n}$ [n = 1, 2: R′ = Et, CH_2Me;[11] Pr^i, $(CHMe_2)$;[12,13] *n*-Bu, $(CH_2)_3Me$;[14] see Figure 1a], not the simple exchange products. Other, sterically varied carboxylic acids (HORc = $HO_2C(\mu_3\text{-}C)[Co_3(CO)_9]$ ($HOAcCo_3$), $HO_2CC(Me)=CH_2$ (HOMc), and HO_2CH (HOFc)) have also been investigated, and additional structural types have been isolated (Figure 1a−f).[1, 16−20]

Currently, too many variables (both chemical and physical) exist to realistically determine the controlling aspects for the densification of the final films of the complex ceramics (i.e., $Pb(Zr,Ti)O_3$)[21−23] that use these precursors. Therefore, we choose to use TiO_2 as a model for these multicationic ceramic materials since it is a single-component ceramic, but also due to the fact that a great deal of interest currently exists for thin films of TiO_2 with controlled densities. Recent applications of TiO_2 thin films include catalysts,[24,25] sensors,[26−28] membranes,[29−32] coatings,[33−36] and electrochromic[37−40] devices.

Carrying out a systematic investigation of $Ti(OR)_4$ precursors and their effect on TiO_2 thin films requires a well-characterized family of similarly ligated compounds in both solution and solid state. In comparison to the $Ti(OR)_4$ family of M_4O_{16} structurally characterized species (R = Me;[41] Et;[42] THME[43]), HORc (see Table 1)-modified $Ti(OPr^i)_4$ compounds are more stable to hydrolysis and possess structurally diverse family members, such

(9) Day, V. W.; Eberspacher, T. A.; Klemperer, W. G.; Park, C. W. *J. Am. Chem. Soc.* **1993**, *115*, 8469.
(10) Boyle, T. J.; Bradley, D. C.; Hampden-Smith, M. J.; Patel, A.; Ziller, J. W. *Inorg. Chem.* **1995**, *34*, 5893.
(11) Gautier-Luneau, I.; Mosset, A.; Galy, J. *Z. Kristallogr.* **1987**, *180*, 83.
(12) Doeuff, S.; Dromzee, Y.; Sanchez, C. *C. R. Acad. Sci. Paris* **1989**, *308*, 1409.
(13) Doeuff, S.; Dromzee, Y.; Taulelle, F.; Sanchez, C. *Inorg. Chem.* **1989**, *28*, 4439.
(14) Laaziz, I.; Larbot, A.; Guizard, C.; Durand, J.; Cot, L.; Joffre, J. *Acta Crystallogr., C (Cryst. Struct. Commun.)* **1990**, *46*, 2332.
(15) Boyle, T. J.; Alam, T. A.; Dimos, D.; Moore, G. J.; Buchheit, C. D.; Al-Shareef, H. N.; Mechenbier, E. R.; Bear, B. R. *Chem. Mater.* **1997**, *9*, 3187.
(16) Boyle, T. J.; Tafoya, C. J.; Scott, B. L. *Abstracts of Papers*, 211th National Meeting of the American Chemical Society, New Orleans, LA, Spring 1996; American Chemical Society: Washington, DC, 1996; Part 1, INOR-62.
(17) Lei, X.; Shang, M.; Fehlner, T. P. *Organometallics* **1997**, *16*, 5289.
(18) Schubert, U.; Arpac, E.; Glaubitt, W.; Helmerich, A.; Chau, C. *Chem. Mater.* **1992**, *4*, 291.
(19) Kickelbick, G.; Schubert, U. *Eur. J. Inorg. Chem.* **1998**, 159.
(20) Boyle, T. J.; Alam, T. M.; Tafoya, C. J.; Scott, B. L. *Inorg. Chem.* **1998**, *37*, 5588.
(21) Boyle, T. J.; Dimos, D. B.; Alam, T. M.; Schwartz, R. W.; Buchheit, C. D.; Sinclair, M. B. *J. Mater. Res.* **1997**, *12*, 1022.
(22) Schwartz, R. W.; Assink, R. A.; Headley, T. J. *Mater. Res. Soc. Symp. Proc.* **1992**, *243*, 245.
(23) Schwartz, R. W.; Boyle, T. J.; Lockwood, S. J.; Sinclair, M. B.; Dimos, D.; Buchheit, C. D. *Integr. Ferroelectr.* **1995**, *7*, 259.
(24) Valden, M.; Pak, S.; Lai, X.; Goodman, D. W. *Catal. Lett.* **1998**, *56*, 7.
(25) Walton, R. M.; Liu, H.; Gland, J. L.; Schwank, J. W. *Sens. Actuators B−Chem.* **1997**, *41*, 143.
(26) Li, M. W.; Chen, Y. F. *Ferroelectrics* **1997**, *195*, 149.
(27) Atashbar, M. Z.; Sun, H. T.; Gong, B.; Wlodarski, W.; Lamb, R. *Thin Solid Films* **1998**, *326*, 238.
(28) Atashbar, M. Z.; Wlodarski, W. *J. Intell. Mater. Syst. Struct.* **1997**, *8*, 953.
(29) Negishi, N.; Takeuchi, K. *Mater. Lett.* **1999**, *38*, 150.
(30) Baskaran, S.; Song, L.; Liu, J.; Chen, Y. L.; Graff, G. L. *J. Am. Ceram. Soc.* **1998**, *81*, 401.
(31) Peng, D. K.; Yang, P. H.; Liu, Z. T.; Meng, G. Y. *Chem. J. Chin. Univ.-Chin.* **1997**, *18*, 499.
(32) Kikuchi, Y.; Sunada, K.; Iyoda, T.; Hashimoto, K.; Fujishima, A. *J. Photochem. Photobiol.* **1997**, *106*, 51.
(33) Baskaran, S.; Song, L.; Liu, J.; Chen, Y. L.; Graff, G. L. *J. Am. Ceram. Soc.* **1998**, *81*, 401.
(34) Wang, X. R.; Masumoto, H.; Someno, T.; Hirai, T. *J. Jpn. Inst. Metals* **1998**, *62*, 1069.
(35) Martinet, C.; Paillard, V.; Gagnaire, A.; Joseph, J. *J. Non-Cryst. Solids* **1997**, *216*, 77.
(36) Leprincewant, Y.; Yuzhang, K.; Van, V. N.; Souche, D.; Rivory, J. *Thin Solid Films* **1997**, *307*, 38.
(37) Campus, F.; Bonhote, P.; Gratzel, M.; Heinen, S.; Walder, L. *Sol. Energy Mater. Sol. Cells* **1999**, *56*, 281.
(38) Vink, T. J.; Boonekamp, E. P.; Verbeek, R. G. F. A.; Tamminga, Y. *J. Appl. Phys.* **1999**, *85*, 1540.
(39) von Rottkay, K.; Richardson, T.; Rubin, M.; Slack, J.; Kullman, L. *Solid State Ionics* **1998**, *115*, 425.
(40) Kullman, L.; Azens, A.; Granqvist, C. G. *J. Appl. Phys.* **1997**, *81*, 8002.
(41) Wright, D. A.; Williams, D. A. *Acta Crystallogr., Sect. B* **1968**, *24*, 1107.
(42) Ibers, J. A. *Nature (London)* **1963**, *197*, 686.
(43) Boyle, T. J.; Schwartz, R. W.; Doedens, R. J.; Ziller, J. W. *Inorg. Chem.* **1995**, *34*, 1110.

Table 1. Carboxylic Acid (HORc) Precursor Data

Acid (Abbreviation)	Formula (MW) pH[a]	Structure
Formic (HOFc)	CH_2O_2 (46.03) 2.04	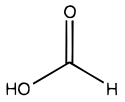
Acetic (HOAc)	$C_2H_4O_2$ (60.05) 2.25	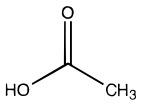
iso-Butyric (HOPc)	$C_4H_8O_2$ (88.11) 2.57	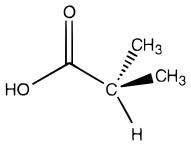
Trimethyl Acetic (HOBc)	$C_5H_{10}O_2$ (102.13) 2.90	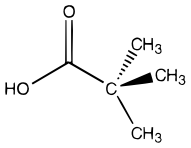
tert-Butyl Acetic (HONc)	$C_6H_{12}O_2$ (116.16) 2.93	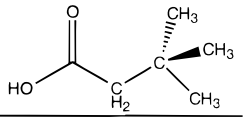

[a] Obtained by pH measurement of an ~1.0 M solution of each HORc in deionized water.

as $Ti_4(O)(OFc)_2(OPr^i)_{10}$ (Figure 1e),[20] $Ti_6(O)_4(OAc)_8(OPr^i)_{12}$ (Figure 1a),[12] $Ti_2(OBc)_2(OPr^i)_6(HOPr^i)$,[16] and $Ti_6(O)_4(ONc)_2(OPr^i)_{12}$ (Figure 1b).[16] To increase the number of useable precursors, we also characterized the HORc (see Table 1)-modified products of $[Ti(\mu\text{-ONep})(ONep)_3]_2$ (**1**)[44] as $Ti_3(O)(OFc)_2(ONep)_8$ (**2**), $Ti_3(O)(OAc)_2(ONep)_8$ (**3**), $Ti_6(O)_6(OPc)_6(ONep)_6$ (**4**), $Ti_2(OBc)_2(ONep)_6$ (**5**), and $Ti_3(O)(ONc)_2(ONep)_8$ (**6**). With these available precursors, investigation of the densification of ceramic thin films (i.e., TiO_2) could be undertaken.[1]

Experimental Section

All of the compounds described below were handled under dry argon or nitrogen atmospheres with rigorous exclusion of air and water using standard Schlenk line and glovebox techniques. FT-IR data were obtained on a Nicolet Magna System Spectrometer-550 using KBr pellets under an atmosphere of flowing nitrogen. TGA/DTA experiments were performed on a Polymer Laboratories STA 1500 Instrument under an atmosphere of flowing oxygen up to 650 °C and at a ramp rate of 5 °C/min. Elemental analyses were performed on a Perkin-Elmer 2400 CHN-S/O elemental analyzer. The changes in film thickness and refractive index at room temperature as a function of drying time were measured by ellipsometry on a Gaertner L116-C ellipsometer.

All NMR samples were prepared from dried crystalline materials that were handled and stored under an argon atmosphere. All $^{13}C\{^1H\}$ solid-state NMR spectra were obtained on a Bruker AMX400 spectrometer at a frequency of 100.63 MHz using a 4-mm broadband magic angle spinning (MAS) probe, spinning at 4 kHz. For all of the $^{13}C\{^1H\}$ cross-polarized (CP) MAS spectra acquired, a standard CP sequence with high-power ^1H decoupling, a 1-ms contact time, and 64−256 scans were utilized. For solution spectra, each sample was redissolved in toluene-d_8 at saturated solution concentrations. All solution spectra were obtained on a Bruker DMX400 spectrometer at 399.87 and 100.54 MHz for ^1H and ^{13}C experiments, respectively. A 5-mm broadband probe was used for all experiments. ^1H NMR spectra were obtained using a direct single-pulse excitation, with a 10-s recycle delay and eight scans on average. The $^{13}C\{^1H\}$ NMR spectra were obtained using a WALTZ-16 composite pulse ^1H decoupling, a 5-s recycle delay, and a $\pi/4$ pulse excitation.

All solvents were freshly distilled from the appropriate drying agent[45] and stored over 4-Å molecular sieves. The following compounds were stored under argon upon receipt (Aldrich) and used without further purification: HONep, HOPc, HOBc, and HONc (see Table 1). HOFc and HOAc were dried over boric anhydride and acetic anhydride/chromium oxide, respectively, and freshly distilled immediately prior to use. $Ti(OPr^i)_4$ was freshly distilled under vacuum immediately prior to use. Compound **1**[44] and the HORc-modified $Ti(OPr^i)_4$ derivatives were prepared as described in the literature.[1,11−13,16] Crystals of $Ti_2(\mu\text{-OBc})(OBc)(OPr^i)_6(HOPr^i)$ (**5a**) and $Ti_6(O)_4(ONc)_4(OPr^i)_{12}$ (**6a**) were isolated by slow evaporation of the toluene reaction mixture of $Ti(OPr^i)_4$ and HOBc or HONc, respectively. Since **2**−**6** were all prepared in an analogous manner, a general synthetic route is described below, with any variations noted in the individual sections.

General Synthesis. To a stirring solution of **1** (1.00 g, 2.52 mmol) in toluene (~5 mL) was added the appropriate HORc (2.52 mmol) in toluene (~1.5 mL) via pipet. After stirring for 12 h, approximately half of the volatile component of the reaction mixture was removed by rotary evaporation. The solution was allowed to sit at glovebox temperatures with slow evaporation of volatile material until crystals formed. The mother liquor was decanted, and the remaining crystals were dried by rotary evaporation. Additional crystalline material was isolated by further slow evaporation of the volatile components.

$Ti_3(O)(OFc)_2(ONep)_8$ (2). HOFc (0.116 g, 2.52 mmol) was used. A white precipitate formed immediately upon addition of HOFc. The reaction was stirred for the amount of time given in the general synthesis procedure, the insoluble material removed by centrifugation, and the soluble fraction allowed to slowly evaporate (vide infra). Crystalline yield: 0.291 g (36.5%). FT-IR (KBr, cm^{-1}): 2956(s), 2905(m), 2869(m), 2844(m), 2732(w), 2692(w), 1595(s), 1561(m), 1479(m), 1462(m), 1394(m), 1372(m) 1366(m), 1259(w), 1216(w), 1080(s,br), 1038(s), 1023(s), 939(w), 905(w), 801(w)772(w), 753(w), 724(m), 679(m, br), 597(m), 538(m). ^1H NMR (tol-d_8, 400.1 MHz): δ 8.48, 8.19 (s, O_2CH), 4.82, 4.51, 4.48, 4.41, 4.40, 4.39, 4.37, 4.36, 4.35, 4.33, 4.29, 4.27, 4.05, 4.02 (s, OCH_2CMe_3) 1.25, 1.09, 1.02, 1.00, 0.79 (s, OCH_2CMe_3). $^{13}C\{^1H\}$ NMR (tol-d_8, 100.6 MHz): δ 168.3, 167.3 (O_2CH), 88.7, 88.1, 86.7, 86.5, 85.0 ($OCHCMe_3$), 34.1, 33.8, 33.5 (OCH_2CMe_3), 27.1, 27.0, 26.9, 26.4, 25.8 (OCH_2CMe_3). Anal. Calcd for $C_{41}H_{89}O_{13}Ti_3$: C, 52.73; H, 9.53. Found: C, 53.03; H, 9.19. TGA/DTA: theoretical weight loss 74.7%, actual 73.2%. Thermal events (°C): 134 (m, endo), 326 (s, exo, recoalescence), 456 (w, exo).

$Ti_3(O)(OAc)_2(ONep)_8$ (3). HOAc (0.152 g, 2.52 mmol) was used. Crystalline yield: 0.700 g (85.1%). FT-IR (KBr, cm^{-1}): 2955(s), 2904(m), 2868(m), 2834(m), 2699(w), 1593(s), 1481(s), 1449(s), 1389(m), 1364(m), 1261(m), 1092(s), 1066(s, sh), 1037(s), 1023(s), 1014(s), 800(m), 751(m), 734(m), 714(m), 694(m, br), 668(m, sh), 631(m), 582(s), 545(w), 502(w). ^1H NMR (tol-d_8, 400.1 MHz): δ 4.79, 4.72, 4.49, 4.46, 4.42, 4.40, 4.38, 4.35, 4.34, 4.32, 4.29, 4.27, 4.26, 4.06, 4.03 (s, OCH_2CMe_3), 2.01, 1.98, 1.81 (s, O_2CMe), 1.26, 1.17, 1.09, 1.07, 1.05, 1.03, 1.01, 0.82 (s, OCH_2CMe_3). $^{13}C\{^1H\}$ NMR (tol-d_8, 100.6 MHz): δ 178.0, 179.9, 177.5 (s, O_2CMe), 90.5, 88.5, 87.8, 86.3, 85.9, 84.6 (OCH_2CMe_3), 35.0, 34.2, 34.0, 33.9, 33.8, 33.5 (OCH_2CMe_3), 27.1, 27.0, 26.9, 26.7, 26.5, 26.5, 25.8, 23.8, 23.5, 22.5 (O_2CMe, OCH_2CMe_3). Anal. Calcd for $C_{44}H_{94}O_{13}Ti_3$: C, 55.93; H, 9.65. Found: C, 55.72; H, 9.31. TGA/DTA: theoretical weight loss 75.4%, actual 70.2%. Thermal events (°C): 128 (w, endo), 154 (w, endo), 317 (s, exo, recoalescence), 456 (w, exo).

$Ti_6(O)_6(OPc)_6(ONep)_6$ (4). HOPc (0.223 g, 2.52 mmol) was used. Crystalline yield: 0.270 g (89.9%). FT-IR (KBr, cm^{-1}): 2954(s), 2905(m), 2867(m), 2837(m), 1570(s), 1540(m), 1473(m), 1428(m), 1393(w), 1363(m), 1263(m), 1095(s, br), 1024(s), 1013(s, sh), 803(m, br), 750(w), 718(m, sh), 698(m, sh), 667(m), 594(w), 526(m). ^1H NMR

(44) Boyle, T. J.; Alam, T. M.; Mechenbeir, E. R.; Scott, B.; Ziller, J. W. *Inorg. Chem.* **1997**, *36*, 3293.

(45) Perrin, D. D.; Armarego, W. L. F. *Purification of Laboratory Chemicals*, 3rd ed.; Pergamon Press: New York, 1988.

(tol-d_8, 400.1 MHz): δ 4.80, 4.63, 4.52, 4.49, 4.45, 4.43, 4.40, 4.37, 4.35, 4.32, 4.28, 4.25, 4.31, 4.05 (s, OCH_2CMe_3), 2.52, 2.42 (sept, O_2CCHMe_2, J_{H-H} = 6.8 Hz) 1.26 (mult, O_2CCHMe_2), 1.18, 1.67, 1.16, 1.15, 1.14 (mult, O_2CCHMe_2) 1.08, 1.03, 1.01, 0.80 (OCH_2CMe_3). $^{13}C\{^1H\}$ NMR (tol-d_8, 100.6 MHz): δ 183.5, 183.4, 183.2, 182.9 (O_2CCHMe_2), 90.1, 88.5, 87.7, 86.1, 85.8, 84.4 (OCH_2CMe_3), 36.4, 36.3 (O_2CCHMe_2), 35.3, 35.0, 34.1, 34.0, 33.9, 33.5 (OCH_2CMe_3), 27.5, 27.1, 26.9, 26.5, 25.8 (OCH_2CMe_3)19.9, 19.5, 19.2, 18.9 (O_2CCHMe_2). Anal. Calcd for $C_{54}H_{108}O_{24}Ti_6$: C, 45.39; H, 7.61. Found: C, 54.27; H, 8.83. TGA/DTA: theoretical weight loss 32.8%, actual 78%. Thermal events (°C): 122 (w, endo), 168 (w, endo), 327 (s, exo, recoalescence), 458 (w, exo).

$[Ti(OBc)(ONep)_3]_2$ (5). HOBc (0.258 g, 2.52 mmol) was used. Crystalline yield: 0.881 g (85.0%). FT-IR (KBr, cm^{-1}): 2954(s), 2904(m), 2866(m), 2844(m), 2695(w), 1559(m, sh), 1532(s), 1480(m), 1415(m), 1391(m), 1375(m), 1360(m), 1305 (w), 1288(w), 1255(w), 1223(m), 1111(s), 1080(s), 1039(m), 1016(m), 933(w), 899(w), 789(m), 746(w), 660(m), 617(m), 600(m), 581(m), 476(m), 464(m). ^1H NMR (tol-d_8, 400.1 MHz): δ 4.82, 4.78, 4.65, 4.62, 4.58, 4.56, 4.52, 4.49, 4.47, 4.44, 4.38, 4.37, 4.35, 4.32, 4.31, 4.29, 4.28, 4.27, 4.26, 4.25, 4.24, 4.23, 4.22, 4.11, 4.09 (s, OCH_2CMe_3), 1.38, 1.35, 1.30, 1.26, 1.25, 1.24, 1.23, 1.20, 1.19, 1.18, 1.17, 1.09, 1.08, 1.07, 1.05, 1.04, 1.03, 1.02, 1.00, 0.99, 0.97, 0.94, 0.76 (s, OCH_2CMe_3, O_2CCMe_3). $^{13}C\{^1H\}$ NMR (tol-d_8, 100.6 MHz, −35 °C): δ 186.8, 185.2, 184.8 (O_2CCMe_3), 88.8, 88.5, 87.5, 87.3, 86.7, 86.1, 85.8, 84.0 (OCH_2CMe_3) 40.1, 39.8, 39.6, 39.3 (OCH_2CMe_3, O_2CCMe_3), 34.5, 34.4, 34.2, 34.0, 33.8 (O_2CCMe_3) 28.2, 28.0, 27.8, 27.6, 27.2, 27.0, 27.0, 26.9, 26.8, 26.7, 25.9 (OCH_2CMe_3). Anal. Calcd for $C_{20}H_{42}O_5Ti$: C, 58.53; H, 10.31. Found: C, 58.73; H, 10.05. TGA/DTA: theoretical weight loss 80.5%, actual 80.7%. Thermal events (°C): 93 (w, endo), 111 (w, endo), 199 (w, endo), 255 (w, exo), 373 (s, exo, recoalescence), 431 (w, exo).

$Ti_3(O)(ONc)_2(ONep)_8$ (6). HONc (0.293 g, 5.05 mmol) was used. Crystalline yield: 0.832 g (90.9%). FT-IR (KBr, cm^{-1}): 2949(s), 2906(m), 2866(m), 2845(m), 1565(s), 1537(m), 1477(m), 1450(m, br), 1409(m), 1391(m), 1362(m), 1092(s), 1070(s), 1037(m), 1022(m), 1009(m), 934(w), 904(w), 798(w), 721(m), 696(m), 668(s), 640(m), 595(m), 542(m), 499(m, br). ^1H NMR (tol-d_8, 400.1 MHz): δ 4.82, 4.68, 4.59, 4.56,4.51, 4.49, 4.48, 4.46, 4.43, 4.40, 4.34,4.32, 4.20, 4.18 (s, OCH_2CMe_3, $O_2CCH_2CMe_3$), 2.35, 1.28, 1.17, 1.15, 1.12, 1.08, 1.06, 1.03 (OCH_2CMe_3, $O_2CCH_2CMe_3$). ^{13}C NMR (tol-d_8, 100.6 MHz): δ 179.4, 179.2 ($O_2CCH_2CMe_3$), 86.5, 87.7, 86.5, 86.3, 84.7 (OCH_2CMe_3), 52.0, 51.5 ($O_2CCH_2CMe_3$), 34.2, 34.0, 33.9, 33.6 (OCH_2CMe_3), 30.6, 30.4, 30.2, 29.7 ($O_2CCH_2CMe_3$), 27.2, 27.0, 26.7, 26.6, 26.4, 25.8 (OCH_2CMe_3, $O_2CCH_2CMe_3$). Anal. Calcd for $C_{52}H_{110}O_{13}Ti_3$: C, 57.46; H, 10.13. Found: C, 57.50; H, 9.78. TGA/DTA: theoretical weight loss 77.9%, actual 80.7%. Thermal events (°C): 86 (w, endo), 134 (w, endo), 156 (w, endo), 338 (s, exo, recoalescence), 434 (w, exo).

X-ray Collection, Structure Determination, and Refinement. Additional details of data collection and structure refinement of the various compounds are given in the Supporting Information. For each structural determination, the respective crystals were handled using standard inert atmosphere oil techniques.

The data for **2**, **4**, **5**, and **6** were collected on a Bruker P4/CCD/PC diffractometer, with a sealed Mo Kα (λ = 0.710 73) X-ray source. A hemisphere of data was collected using a combination of ϕ and ω scans, with 30-s exposures and 0.3° frame widths. Data collection, indexing, and initial cell refinement were handled using SMART software.[46] Frame integration and final cell refinement were carried out using SAINT software.[47] The final cell parameters were determined from a least-squares refinement. The SADABS program was used to perform any absorption corrections.[48] Structures were solved using Direct Methods and difference Fourier techniques. The final refinement included anisotropic temperature factors on all non-hydrogen atoms. Structure solution, refinement, graphics, and creation of publication materials were performed using SHEXTL 5.1 software.[49]

Lattice determination and data collection of **3** were carried out using XSCANS Version 2.10b software.[51] All data reductions, including Lorentz and polarization corrections and structure solution and graphics, were performed using SHELXTL PC Version 4.2/360 software.[52] The structure refinement was performed using SHELX 93 software.[52] The data were not corrected for absorption due to the low adsorption coefficient. The structure was solved using Patterson and difference Fourier techniques.

For **5a** and **6a**, a crystal of each was mounted on a glass fiber and transferred to the cold stream of a Siemens P4 rotating-anode diffractometer. The determination of Laue symmetry, crystal class, unit cell parameters, and the crystal's orientation matrix were carried out according to standard XSCANS procedures.[51] Intensity data were collected at 158 K using a $2\theta-\omega$ scan technique with Mo Kα radiation. The raw data were processed with a local version of CARESS[50] that employs a modified version of the Lehman−Larsen algorithm to obtain intensities and standard deviations from the measured 96-step peak profiles. All data were corrected for Lorentz and polarization effects and were placed on an approximately absolute scale. All calculations were carried out using the SHELXL program.[52] The analytical scattering factors for neutral atoms were used throughout the analysis.[53] The structure was solved by direct methods and refined on F^2 by full-matrix least-squares techniques.

Film Precursor Solutions. Each of the above precursors (**2**−**6**) was individually dissolved in toluene (0.2 M solution) and then transferred to a glass syringe. Under a nitrogen atmosphere (<15% relative humidity), the solutions were filter (2 μm)-deposited onto cleaned silicon wafers (12 mm^2) and spun at 3000 rpm for 30 s. Two samples (films A and B) were generated from each precursor solution. *Film A:* Film A was immediately placed on a hot plate at 100 °C for 60 s and then transferred to the ellipsometer. Refractive indices were measured using the ellipsometer, and then the sample was transferred to a furnace and fired under ambient atmosphere at 450 °C for 60 min. Refractive indices were again measured to determine the densification of the final film. *Film B:* Refractive indices, monitored at regular intervals over a 60-min period, were recorded for film B while it air-dried (25 °C). After this time the sample was fired under conditions identical to those noted for film A, and the refractive indices were again obtained.

Results and Discussion

Schematic representations of the structure types previously identified for HORc-modified $Ti(OR)_4$ are shown in Figure 1a−f.[11−14,16−18,20] We were interested in the structural changes that occurred for HORc-modified $Ti(OR)_4$ using the ONep alkoxide ligand. Furthermore, it was of interest to study how these subtle structural changes would alter the densification of TiO_2 thin films. To accomplish this, it was necessary to identify these compounds in both the solid state and the solution state before investigating the densification of thin films generated from solutions of these compounds.

Synthesis. The products of the stoichiometric reaction (1:1 titanium to HORc, eqs 1−5) were all isolated in a similar manner, wherein, compound **1** was dissolved in toluene and

(46) SMART Version 4.210; Bruker Analytical X-ray Systems Inc., 6300 Enterprise Lane, Madison, WI 53719, 1997.

(47) SAINT Software Users Guide, Version 4.05; Bruker Analytical X-ray Systems, 6300 Enterprise Lane, Madison, WI 53719, 1997.

(48) Sheldrick, G. M. SADABS; Brucker Analytical X-ray Systems, Inc.: Madison WI, 1997.

(49) XSCANS and SHELXTL PC are products of Siemens Analytical X-ray Instruments, Inc., 6300 Enterprise Lane, Madison, WI 53719. (a) SHELX-93 is a program for crystal structure refinement written by G. M. Sheldrick, University Of Göttingen, Germany, 1993. (b) SHELXTL PC Version 4.2/360; Bruker Analytical X-ray Instruments, Inc., Madison, WI 53719, 1994. (c) SHELXTL Version 5.1; Bruker Analytical X-ray Systems, 6300 Enterprise Lane, Madison, WI 53719, 1997.

(50) Broach, R. W. CARESS; Argonne National Laboratory: Argonne, IL, 1978.

(51) XSCANS Software Users Guide, Version 2.1; Siemens Industrial Automation, Inc.: Madison, WI, 1994

(52) Sheldrick, G. M. SHELXL; Siemens Analytical X-ray Instruments, Inc.: Madison WI, 1994

(53) *International Tables for X-ray Crystallography*; Kluwer Academic Publishers: Dordrecht, The Netherlands, 1992; Vol. C.

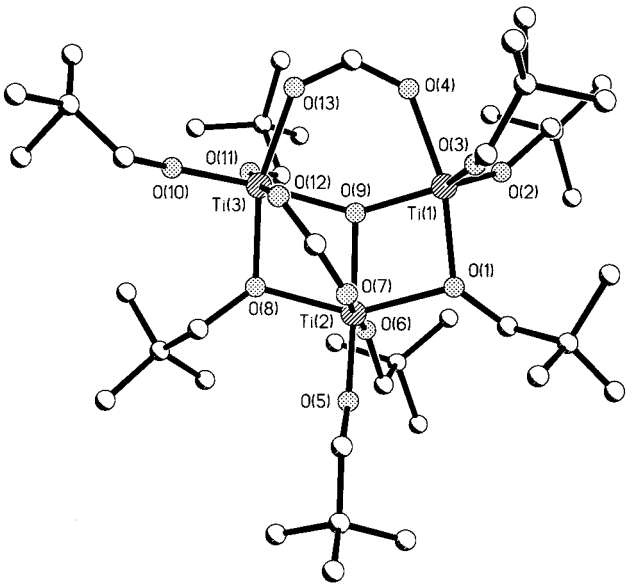

Figure 2. Ball-and-stick plot of **2**.

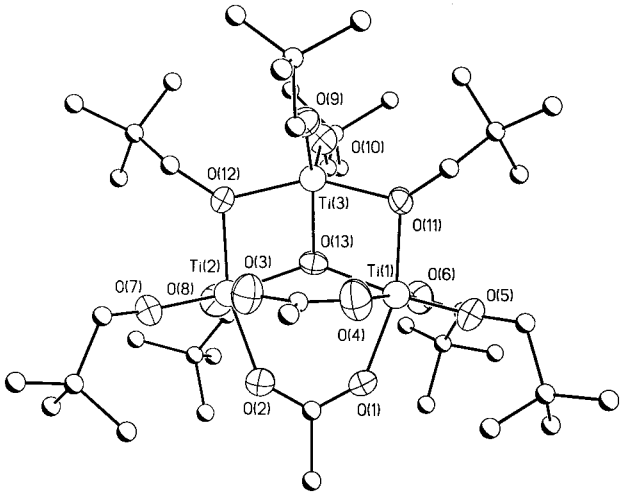

Figure 3. Thermal ellipsoid plot of **3**. Thermal ellipsoid plots are drawn at the 50% level.

the appropriate HORc reagent was added with stirring. Crystals of **2**−**6** were isolated by slow evaporation of the volatile material from the reaction mixture as described in the Experimental Section. Figures 2−6 are the thermal ellipsoid plots of **2**−**6**, respectively.

$$[\mathrm{Ti}(\mu\text{-ONep})(\mathrm{ONep})_3]_2 + 2\mathrm{HOFc} \xrightarrow{\text{toluene}} {}^2/_3\mathrm{Ti}_3(\mathrm{O})(\mathrm{OFc})_2(\mathrm{ONep})_8 \quad (1)$$

$$[\mathrm{Ti}(\mu\text{-ONep})(\mathrm{ONep})_3]_2 + 2\mathrm{HOAc} \xrightarrow{\text{toluene}} {}^2/_3\mathrm{Ti}_3(\mathrm{O})(\mathrm{OAc})_2(\mathrm{ONep})_8 \quad (2)$$

$$[\mathrm{Ti}(\mu\text{-ONep})(\mathrm{ONep})_3]_2 + 2\mathrm{HOPc} \xrightarrow{\text{toluene}} {}^1/_3\mathrm{Ti}_6(\mathrm{O})_6(\mathrm{OPc})_6(\mathrm{ONep})_6 \quad (3)$$

$$[\mathrm{Ti}(\mu\text{-ONep})(\mathrm{ONep})_3]_2 + 2\mathrm{HOBc} \xrightarrow{\text{toluene}} [\mathrm{Ti}(\mathrm{OBc})(\mathrm{ONep})_3]_2 \quad (4)$$

$$[\mathrm{Ti}(\mu\text{-ONep})(\mathrm{ONep})_3]_2 + 2\mathrm{HONc} \xrightarrow{\text{toluene}} {}^2/_3\mathrm{Ti}_3(\mathrm{O})(\mathrm{ONc})_2(\mathrm{ONep})_8 \quad (5)$$

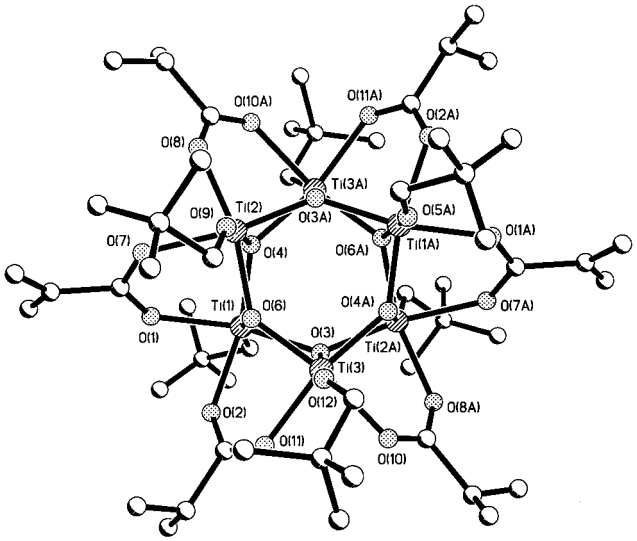

Figure 4. Ball-and-stick plot of **4**.

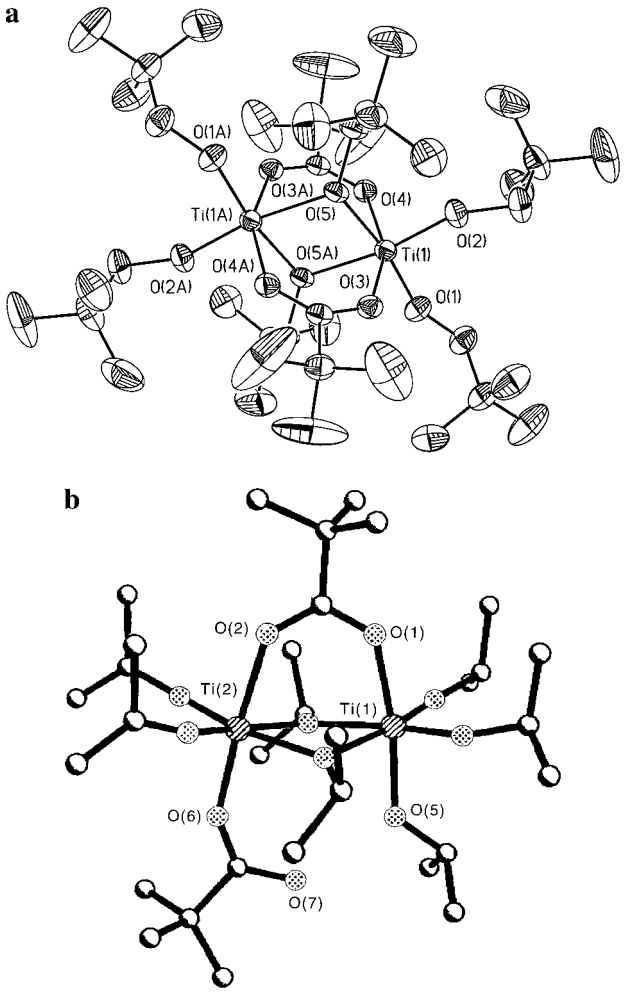

Figure 5. (a) Thermal ellipsoid plot of **5** and (b) ball-and-stick plot of **5a**. Thermal ellipsoid plots are drawn at the 50% level.

In the literature, the origin of the oxo ligand has been attributed to either an etherification[17] or an esterification[1,11−14,16,18−20] mechanism. For simple organic acid modifiers, esters have been identified as the main byproducts.[1,11−14,16,18−20] For eqs 1−5, the byproducts were not fully investigated; however, due to the similarities of the previous reports, an esterification pathway is the most likely mechanism for the production of the oxo ligands. The rapidity with which oxolation

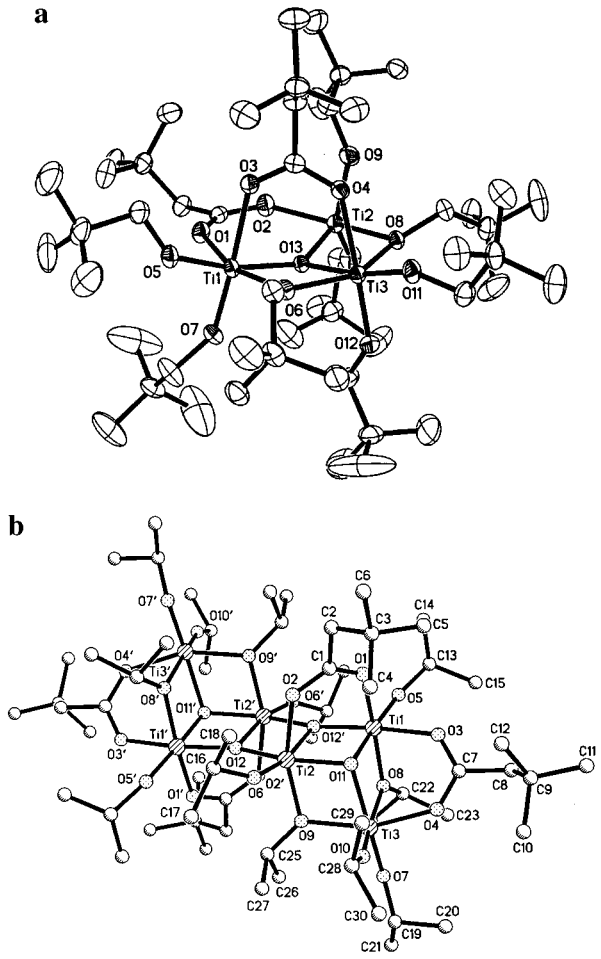

Figure 6. (a) Thermal ellipsoid plot of **6** and (b) ball-and-stick plot of **6a**. Thermal ellipsoid plots are drawn at the 50% level.

Table 2. Properties of Compounds **1**−**6**: Degree of Condensation (*x*/*y*), Maximum Molarity (M_{max}), and Sublimation (T_{sub}), Decomposition (T_{dec}), and Crystallization (T_{cry}) Temperatures

compd	*x*/*y*	∼M_{max} (g/mL)	∼T_{sub}[a] (°C)	∼T_{dec} (°C)	∼T_{cry} (°C)	ref
1	0.0	>2.5	90			44
2	0.33	0.36	130	326	456	*b*
3	0.33	0.35	130	317	456	*b*
4	1.0	0.76	155	342	489	*b*
5	0.0	0.27	100	328	431	*b*
6	0.33	0.49	135	338	434	*b*

[a] Sublimation performed at 10^{-4} Torr. [b] This work.

occurs under the very mild conditions investigated in this study suggests that the hydrophilic Ti metal center acts as a catalyst for the esterification reaction. As evidenced by the structural variations isolated in these systems, the choice of solvent, alkoxide group, and acid will dictate the rate and extent of reaction (i.e., water formation and subsequent hydrolysis) that ultimately dictate the final product composition. Under the conditions presented here, we can reproducibly generate **2**−**6** from an assumed esterification mechanism.

Table 2 shows the solubility limit determined and the various temperatures of sublimation and crystallization of the ceramic phase (as determined by TGA/DTA) for **2**−**6**. One trend noted in the TGA/DTA data was that, as the molecules become more condensed and thus more stable, the decomposition temperature and crystallization temperatures increased. The elemental analyses and TGA/DTA data for **2**−**6** were consistent for each compound, expect for **4**. While this suggests that the bulk powder of **4** is not consistent with the X-ray structure, numerous crystals were solved, and all proved to have structures identical to that reported for **4**.

Since the ONep stretches dominate the FT-IR spectra of **2**−**6**, it is reasonable to focus on the HORc (>1500 cm^{-1}) and M−O (<700 cm^{-1}) stretching frequency regions[2] to discern solid-state structural differences. For each compound, the carbonyl stretch of the ORc ligand is shifted, indicating a bidentate ligation. A stretch around 530 cm^{-1} was present in the spectra of **2**, **3**, **4**, **6**, and the other HORc-modified complexes but was absent in the spectrum of **5**. This was assigned as the Ti−(μ_3-O) stretch. FT-IR spectra obtained on samples of **2**−**6** that had been exposed to room-temperature atmospheric conditions (20−25% relative humidity) for >2 h were unchanged, except for **5**. The relative instability of **5** to hydrolysis versus the other HORc-modified $Ti(OR)_4$ compounds must be a reflection of the reduced oxolation. Each complex was successfully sublimed <175 °C (10^{-3} Torr); however, the FT-IR spectrum recorded for the sublimed material was altered in comparison to the starting spectrum of each precursor. This indicates that further reactivity of **2**−**6** can be expected with either gas-phase reactions or heating of the samples. The saturation solubility of these compounds varied from 0.22 to 0.49 M, wherein the larger pendant hydrocarbon chains of the HORc yielded higher molarities. The exception is the unesterified OBc derivative, **5**, which, quite surprisingly, demonstrated the lowest solubility.

Solution- and Solid-State Characterization. To interpret the information garnered from these compounds concerning the densification of TiO_2 thin films, it was critical that the solution behavior (nuclearity) of each compound be determined. Due to the complexity of the solution data associated with metal alkoxides, it was first necessary to identify these compounds in the solid state. Solid-state NMR was used to verify that the bulk powders were consistent with the single-crystal X-ray studies.

(a) Solid State. The skeletal arrangements of known $Ti(O)_w(ORc)_x(OR)_y$ compounds are shown in Figure 1. The basic structural arrangements of this family of compounds are best described as $[Ti-O]_4$ cubes with different corners removed or reflected. The thermal ellipsoid plots of **2**−**6** are shown in Figures 2−6, respectively. A complete listing of the single-crystal X-ray data collection parameters for **2**−**6** can be found in the Supporting Information. The *R*1 value for every structure was below 10%, except for **4** (12.77%) and **5a** (10.92%).

Compounds **2**, **3**, and **6** adopt a unique dual corner-missing cube structural arrangement (Figure 1g) observed for HORc-modified $Ti(OR)_4$ compounds. For each structure, the three Ti metal centers are linked by a μ_3-O ligand. The remainder of the structures are an asymmetric (**2** and **6**) or symmetric (**3**) assemblage of bridging and terminal ligands, as determined by the placement of the ORc ligand. In comparison to the analogous OPr^i derivatives $[Ti_4(O)_2(OFc)_2(OPr^i)_{10}$ (Figure 1e),[20] $Ti_6(O)_4(OAc)_4(OPr^i)_{12}$ (Figure 1a),[12] and $Ti_6(O)_4(ONc)_4(OPr^i)_{12}$ (**6a**, Figure 1b)[16]], the introduction of the ONep ligand significantly reduces the nuclearity of the resultant HORc-modified $Ti(OR)_4$ compounds.

Figure 4 is the thermal ellipsoid plot of **4**. This is only the second known modified alkoxide to adopt the hexagon-prismatic structure (Figure 1f),[20] which consists of two offset $[Ti-O]_3$ rings stacked on top of each other. No structure has been reported for the OPr^i/OPc derivative. Several crystals of **4** were analyzed, but all proved to have a partial atom in a 90 °C rotation to the hexagon-prism.

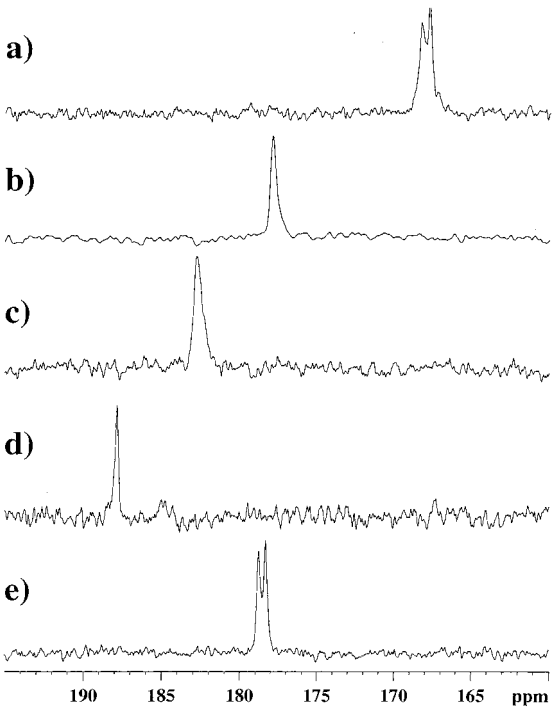

Figure 7. Stacked plot of the ^{13}C NMR spectra of the carboxylic region of **2**−**6** (a−e).

The OBc derivative, **5** (Figure 5a), represents the first report of a noncondensed, fully exchanged, titanium alkoxy acetate structure. There is *no* oxo ligand present. In comparison, the only other noncondensed structure was reported for $Ti_2(\mu$-OBc)-(OBc)$(OPr^i)_6(HOPr^i)$ (**5a**, Figure 5b).[16] The coordinated acid and alcohol share a proton in what can be considered the first step in the formation of esterification products. Compounds **5** and **5a** represent a novel set of HORc-modified $Ti(OR)_4$ compounds. The large, sterically hindering OBc acid dictates the formation of simple exchange products, such as **5**. By altering the pendant hydrocarbon chain of the alkoxy ligand, the intermediate **5a** was formed. Therefore, judicious choice of both the acid and alkoxide ligands could lead to a wide range of compounds at various stages of reactivity.The bond distances and angles of **2**−**6**, **5a**, and **6a** were consistent with each other and literature reports, wherein (i) the higher the degree of binding the ligand undergoes, the longer the Ti−O bond distances ($Ti-OR_{term}$ < $Ti-(\mu$-OR) < $Ti(-(\mu_3$-OR)) and (ii) the five- and six-coordinated metal centers adopt trigonal bipyramidal and octahedral geometries, respectively. One notable variation was observed for the five-coordinated Ti metal center of **6**, which was isolated in an unusual distorted square-base geometry.

To further characterize the bulk powders of **2**−**6**, solid-state NMR experiments were undertaken. Crystalline material of each compound was dried in vacuo, packed into rotors, and stored under an argon atmosphere until immediately prior to obtaining a ^{13}C CP-MAS NMR spectrum. A stacked plot of the ^{13}C NMR spectra of the carboxylic carbon region of **2**−**6** is shown in Figure 7. Since few solid-state NMR spectra are reported for these types of compounds, it is difficult to know if the numerous disorders and inequivalancies observed for **2**−**6** are typical; however, we have interpreted the observed spectra on the basis of their solid-state structures.

For **2**, **3**, and **6**, the resonances recorded for the respective CP-MAS spectra are insufficiently resolved to allow for unambiguous determination of the bulk powder structure. The reduction in the number of methylene and methyl resonances observed for the pendant hydrocarbon chains, in comparison with their respective solid-state structures, can be accounted for by coincidental overlap of similar ligands. Due to the uniqueness of the carboxylic carbon (O_2CR) resonances in these compounds, this region was used for structural interpretation (Figure 7).

For **2** and **6**, the solid-state structure is asymmetric, yielding two disparate ORc ligands which were observed in the solid-state ^{13}C spectra. In contrast, the symmetric **3** revealed only one type of ORc carbon resonance. For the symmetrical, hexagon-prism shape of **4**, only a single type of OPc was recorded which is consistent with the solid-state structure; however, the two sets of ONep resonances observed most likely reflect the disorder noted in the crystal structure. The dinuclear OBc complex, **5**, displays only one type of OBc carbon, as expected. The large number of methyl ONep peaks also recorded can be explained as packing inequivalencies of the pendant chains in the solid state. Based upon the carboxylate resonances, the bulk powders of the crystalline materials of **2**−**6** are consistent with their respective X-ray structures.

(b) Solution State. Since the TiO_2 thin films were to be generated from solution methods, it was therefore necessary to understand the solution behavior of **2**−**6** (i.e., were the solid-state structures retained in solution?). Hence, solution-state NMR studies were undertaken using crystalline samples of **2**−**6** that were dried in vacuo, redissolved in cold toluene-d_8, and immediately inserted into a cold (−35 °C) probe. This experimental setup was utilized to minimize the degree of self-esterification that similar compounds have been reported to undergo.[20] All of the samples displayed the same room-temperature NMR spectrum originally obtained for that sample after high-temperature VT-NMR investigations. No ester formation was observed for these compounds.One figure of merit that has been postulated to determine the stability of titanium oxo compounds in solution involves calculating the degree of condensation (x/y, where x = number of oxo ligands and y = number of metal cations).[17,20,54] However, this must be tempered with the "amount of openness" displayed by the various molecules.[17,20,54] For **2**, **3**, and **6**, x/y = 0.33, and these compounds adopt a somewhat "closed structure". This suggests that these compounds may demonstrate fluxional behavior in solution. For **5**, x/y = 0, and the similarity in structure to that of **1** suggests that dynamic behavior should be observed for this compound. For **4**, the x/y = 1, coupled with the low degree of "openness", suggests that the structure of **4** should be stable in solution. These concepts were used to aid in interpreting the solution behavior of **2**−**6**. The asymmetric compound of **2** displayed two types of OFc shifts in both the VT-NMR ^{1}H and ^{13}C NMR spectra, independent of the temperature or concentration studied. There are a number of resonances present for the ONep ligands that coalesce upon warming. This indicates that the central core of **2** is retained on the NMR time scale with a great deal of dynamic ligand behavior that is often associated with metal alkoxide complexes. The similarly structured **6** has a solution spectrum that reveals a more symmetric molecule in solution at room temperature since only one ONc carboxylic carbon can be observed. Again, a great deal of dynamic behavior associated with the ONep ligands was noted as resonances in the spectrum coalesced with increasing temperature. On the other hand, the ^{1}H NMR spectrum of **2** shows a great deal of asymmetry at low temperatures. At higher temperatures (50 °C), only one type of OAc carboxylate resonance was observed. It is easily envisioned that the symmetric and asymmetric struc-

(54) Day, V. W.; Eberspacher, T. A.; Chen, Y.; Hao, J.; Klemperer, W. G. *Inorg. Chim. Acta* **1995**, *229*, 391.

Table 3. Film Properties of 0.2 M Solutions of **1**−**6** for Sintered Films

compd	av thickness (Å) green	av thickness (Å) sintered	η_f (av)[a]	$\rho_{normalized}$ (av)[b]	ref
1	388	212	2.13	99.0	*c*
2	344	199	2.19	102	*c*
3	435	232	2.17	101	*c*
4	330	151	2.10	97.0	*c*
5	819	273	1.92	86.5	*c*
6	793	281	1.94	87.5	*c*
$Ti(OPr^i)_4$	361	218	2.113	97.95	1, 16, *c*
$Ti_4(O)_2(OFc)_2(OPr^i)_8$	345	186	2.170	100.7	1, 16, *c*
$Ti_6(O)_4(OAc)_4(OPr^i)_{12}$	312	101	2.038	93.65	1, 16, *c*
$Ti(OPr^i)_4$/HOPc	400	183	2.082	96.20	1, 16, *c*
$Ti_2(OBc)_2(OPr^i)_6(HOPr^i)$	1028	316	1.802	78.26	1, 16, *c*
$Ti_6(O)_4(ONc)_4(OPr^i)_{12}$	556	222	1.9660	89.24	1, 16, *c*

[a] Index of refraction. Average determined by a point-to-point sampling of at least two thin films. [b] Normalized density. Average determined by a point-to-point sampling of at least two thin films.[c] This work.

tures noted for **2**, **3**, and **6** are easily intertransformed by simple ligand rearrangement. However, even with the rearrangement noted for the individual compounds (**2**, **3**, and **6**), based upon the low number of ORc resonances present, it appears that the central core of these compounds is preserved in solution.

For the solid-state disorder structure of **4**, the solution-state NMR spectra at low temperature (−40 °C) are very complex. This may represent inequivalencies based upon reduced dynamic ligand exchange or further indications of the disorder noted for this molecule. At higher temperatures, the resonances coalesce to form only one type of OPc ligand and two types of ONep ligands. Based on the symmetry adopted by **4** at higher temperatures and the stability of the OFc/OPr^i derivative,[20] the general constructs of **4** appear to be maintained in solution.

For **5**, more resonances than can be accounted for from the solid-state structure are present through out the VT-NMR experiments investigated. The changes in resonances that were noted could not be accounted for by simple ligand rearrangement. Therefore, molecular weight determinations were undertaken using the Signer method[55] to further clarify the solution behavior of **5**. This study revealed that **5** had a solution molecular weight of 1005 or a nuclearity of ∼1.23 in comparison to the solid-state structure of **5**. These data indicate that **5** maintains its primary dinuclear structure with some equilibrium involving higher order species.

Film Properties. Since the solid-state structures are maintained to a great extent in solution, interpretation of the resultant changes in the densification of the thin films of TiO_2 can be based upon the structural variations noted for **2**−**6** (vide supra). Under an atmosphere of argon, an ∼0.2 M toluene solution was generated for each sample and transferred to a glass syringe. Films were generated under a controlled nitrogen atmosphere (<15% relative humidity) to minimize hydrolysis. Two films were generated for each sample, and the use of a timer was initiated to maintain a systematic investigation. Properties of the final films are listed in Table 3.

The first film was transferred directly to an ellipsometer, and a drying pattern was recorded by measuring the index of refraction (η_f) and thickness (in angstroms). For every sample (**1**−**6**), a standard drying curve was noted. All of the films dried to an average thickness of 223(46) Å (range 143−270 Å) within a 1-h period.

The second film was placed on the stage of an ellipsometer to determine initial film thickness. After this measurement, the film was immediately placed into a preheated furnace and sintered at 450 °C to form TiO_2. Each sample had thickness values similar to those recorded for the first films. The final η_f and thicknesses were recorded for each film (see Table 3). Normalized density ($\rho_{normalized}$) calculations were determined using the Lorentz−Lorentz equation, eq 6.[56]

$$\rho_{normalized} = \frac{[(n_f^2 - 1)(n_a^2 + 2)]}{[(n_f^2 + 2)(n_a^2 - 1)]} \quad (6)$$

n_f = film index of refraction

n_a = anatase index of refraction

It was determined that the samples with ∼100% density are the low-carbon-containing carboxylate, corner-missing, shaped (Figure 1g) molecules with an *x*/*y* ratio of 0.3 or lower (**2** and **3**). The high density of these films can be explained by the "cross-linking" properties of these precursors and their low nuclearity. Cross-linking, or the formation of M−O−M bonds, is directly related to the ability of the terminal OR to be hydrolyzed. The introduction of the bidentate ORc ligands has a two-fold effect on the cross-linking ability of a molecule. The steric bulk of the ORc ligand "protects" the metal center from hydrolysis, but, more importantly, there is a reduction in the number of terminal OR ligands. This limits the direction in which cross-linking can occur. Hence, uniform (or controlled) hydrolysis yields controlled cross-linking, thus limiting voids. This effect should be observed for large and small nuclearity compounds, and both should yield dense films. However, smaller molecules would have fewer sites of reactivity per molecule, and the resulting controlled cross-linking would be greater, yielding films with fewer voids.

The thin film of **1** is almost 100% dense, possibly due to partial hydrolysis by the remnant humidity in the box (**1** has been reported to adopt a $Ti_{12}(O)_{16}(ONep)_{32}$ structure upon full hydrolysis)[16] that leads to compounds similar to those observed for **2** and **3**. Compound **4** also had a high density, and an argument similar to that made for **2** and **3** would be valid; however, due to the general shape of **4**, increased void inclusion would be expected, and thus a lower density film should result.

Compounds **5** and **6** also possess some of the characteristics described above for the production of highly dense films; however, the densities of their resultant films do not exceed 88%. Therefore, the amount of organic constituent of the HORc chain must *also* play a determining role in densification of the final thin film. One interpretation that can be inferred is that the larger ligands generate more organic decomposition gases. The need to eliminate the increased amount of byproduct may overwhelm the ability of these smaller molecules to densify, resulting in voids. From the ellipsometric data collected for **2**−**6**, it is readily apparent that a fine balance between oxo ligands and carbon content of the HORc must be maintained to optimize densification of the final film.

If lower nuclearity and lower carbon content are valid characteristics for generating highly dense films, then the OPr^i derivatives, which have higher nuclearity than their ONep counterparts, should yield less dense films. Therefore, thin films of the OPr^i derivatives were investigated in a manner similar to that presented for the ONep compounds. Table 3 tabulates the final results of the films generated using the OPr^i-ligated species.

(55) Clark, E. P. *Analytical Ed.* **1941**, 820.

(56) Born, M.; Wolf, E. *Principles of Optics*; Permagon Press: New York, 1975; p 87.

The smaller nuclei ONep compounds were, on average, thicker than the OPr^i films both as the "green" (unfired) and as sintered films. The densities of the final films, based on the η_f, indicate that the ONep-ligated species were more dense. Furthermore, higher initial carbon content of the OPr^i species also appears to result in a further decrease in the density of the sintered films. Again, the high densities of the TiO_2 thin films generated from $Ti(OPr^i)_4$ are most likely a result of hydrolysis from residual humidity in the glovebox, forming a partially condensed species.

Conclusion

We have synthesized and characterized several new members of the HORc-modified $Ti(OR)_4$ family. These compounds were synthesized through the reaction of HORc and **1** and identified by single-crystal X-ray diffraction as $Ti_3(O)(OFc)_2(ONep)_8$, $Ti_3(O)(OAc)_2(ONep)_8$, $Ti_6(O)_6(OPc)_6(ONep)_6$, $[Ti(OBc)(ONep)_3]_2$, and $Ti_3(O)(ONc)_2(ONep)_8$. The novel structures identified in this study for HORc-modified $Ti(OR)_4$ include (i) the first example of trinuclear, oxo, alkoxy, or acetate titanium complex, referred to as a dual corner-missing complex (**2**, **3**, **6**), and (ii) the first "simple" metathesized acetate−alkoxide isolated product (**5**). The bulk samples of **2**−**6** were found to be consistent with their solid-state structures, based on elemental analysis and ^{13}C CP-MAS solid-state NMR spectroscopy. In general, each of the ONep derivatives yields a compound that possesses reduced nuclearity (often halved) in comparison to the OPr^i derivatives. While solution NMR spectroscopy studies of **2**−**6** in toluene reveal a great deal of dynamic behavior associated with ligand exchange and multinuclear equilibria, the general solid-state constructs of **2**−**6** appear to be maintained in solutions. Using the well-characterized species **2**−**6** and their OPr^i analogues in a systematic study of the densification of TiO_2 thin films has allowed for the development of an understanding of the relationship between ligand, precursor structure, and final film properties. The most desirable starting precursors that were found to generate fully dense TiO_2 films have small nuclearities, few terminal alkoxides, and an overall low carbon content. Compounds **2** and **3** demonstrated these properties and generated films of ∼100% densification. Proper exploitation of these characteristics and trends noted for the various precursors will allow for the production of thin films with controlled properties.

Acknowledgment. For support of this research, the authors thank the Office of Basic Energy and Science and the United States Department of Energy, under Contract DE-AC04-94AL85000. Sandia is a multiprogram laboratory operated by Sandia Corporation, a Lockheed Martin Company, for the United States Department of Energy.

Supporting Information Available: X-ray crystallographic files, in CIF format, for the structures of **2**−**6** (**5a** and **6a**). A detailed listing of the crystallographic data collection parameters (PDF). This material is available free of charge via the Internet at http://pubs.acs.org.

JA992521W